

# Real-Time Detection and Classification of Power System Disturbances Based on Maximal Overlap Discrete Wavelet Transform

**Flavio B. Costa**

UFRN  
Natal, Brazil  
flaviocosta@ect.ufrn.br

**Benemar A. Souza**

UFCG  
Campina Grande, Brazil  
benemar@dee.ufcg.edu.br

**Núbia S. D. Brito**

UFCG  
Campina Grande, Brazil  
nubia@dee.ufcg.edu.br

**Abstract** - This paper presents a wavelet-based method for real-time disturbance detection and classification in transmission power systems. Both wavelet and approximation coefficients of the voltages and currents are computed through the maximal overlap discrete wavelet transform, at first scale, by using the pyramid algorithm adapted for real-time. The wavelet and approximation coefficient energies of the voltages and currents are analyzed to detect and classify the disturbances in real-time. The diagnostic method can detect faults and other power system disturbances with transients, such as voltage sags and switching transients. The proposed method was implemented by using the Real Time Digital Simulator (RTDS).

**Keywords** - Real-time fault detection, real-time transient detection, wavelet transform.

## 1 Introduction

Real-time analysis of faults and power quality (PQ) disturbances has become an important issue to electrical utilities in order to minimize the harmful effects of such disturbances and improve system stability. For instance, the real-time detection of fault-induced transients followed by the real-time fault classification and location can provide very fast relay operation in transmission lines. This paper presents a method for real-time detection and identification of faults and other power system disturbances with transients, such as voltage sags and transients due to transmission line energization and de-energization.

Voltages and currents during faults and other power system disturbances with transients are non-stationary in both time and frequency domains with typical frequency spectrum from a few hundred Hz to various kHz [1, 2]. These signals can be properly analyzed by using the discrete wavelet transform (DWT), which is a well-known powerful tool to detect power system transients [3, 4, 5, 6, 7], to detect PQ disturbances [8, 9], to detect and classify faults [10, 11], and to estimate the fault location [12, 13]. However, the wavelet transform can also be used for real-time analysis of faults and PQ disturbances [14]. In real-time applications, transients in faults and PQ disturbances can be detected faster by using the maximal overlap discrete wavelet transform (MODWT) [15, 14], a variant of the DWT [16].

This paper presents a wavelet-based method for real-time disturbance detection and classification in transmission power systems. In order to detect the transients as soon as possible, both wavelet and approximation coeffi-

cients of the voltages and currents are computed through the MODWT, at first scale, by using the pyramid algorithm adapted for real-time. The wavelet and approximation coefficient energies of the voltages and currents are analyzed to detect and identify the disturbances in real-time. The Real-Time Digital Simulator (RTDS) was used in order to evaluate the performance of the proposed method and good results were obtained.

## 2 Real-Time Wavelet Transform

The MODWT uses both low-pass filter ( $g$ ) and high-pass filter ( $h$ ) to divide the frequency-band of the input signal into low-frequency components (approximation coefficients) and high-frequency components (wavelet coefficients) at various scales. There is no down-sampling process in MODWT [16]. As a consequence, the approximation and wavelet coefficients can be computed soon after each sampling process (the disturbances can be detected faster).

The simulation time step of the RTDS is  $\Delta t=50 \mu s$  (sampling frequency  $f_s=20$  kHz). Therefore, the frequency spectra of the approximation and wavelet coefficients at the first scale fall in the ranges  $[0, 5]$  and  $[5, 10]$  kHz, respectively [16]. As a consequence, the wavelet coefficients at the first scale are well-suitable to detect the highest frequency components of the disturbances. On the other hand, the approximation coefficients are mainly influenced by the fundamental power frequency (useful for disturbance identification).

The coefficients of the filter pairs are associated with the selected mother wavelet. The wavelet Daubechies 4 (db4) [17] provides an accurate detection of the fast transients in faults and other power system disturbances [6, 11, 18]. In addition, the four coefficients of the db4 filters provide a fast computation of the wavelet coefficients, an excellent feature for real-time applications.

The MODWT is defined in terms of a computationally efficient pyramid algorithm [16]. Considering the phase A voltage ( $v_A$ ) with length of  $k_t$  samples, the approximation coefficients ( $A$ ) and wavelet coefficients ( $W$ ) of the MODWT pyramid algorithm, at the first scale, with  $g$  and  $h$  which has four coefficients ( $L=4$ ) are given by:

$$A_{v_A} = \begin{bmatrix} g(4) & 0 & 0 & \dots & g(2) & g(3) \\ g(3) & g(4) & 0 & \dots & g(1) & g(2) \\ g(2) & g(3) & g(4) & \dots & 0 & g(1) \\ g(1) & g(2) & g(3) & \dots & 0 & 0 \\ \vdots & \vdots & \vdots & \vdots & \vdots & \vdots \\ 0 & 0 & 0 & \dots & g(3) & g(4) \end{bmatrix} \begin{bmatrix} v_A(1) \\ v_A(2) \\ v_A(3) \\ v_A(4) \\ \vdots \\ v_A(k_t) \end{bmatrix}, \quad (1)$$

$$W_{v_A} = \begin{bmatrix} h(4) & 0 & 0 & \dots & h(2) & h(3) \\ h(3) & h(4) & 0 & \dots & h(1) & h(2) \\ h(2) & h(3) & h(4) & \dots & 0 & h(1) \\ h(1) & h(2) & h(3) & \dots & 0 & 0 \\ \vdots & \vdots & \vdots & \vdots & \vdots & \vdots \\ 0 & 0 & 0 & \dots & h(3) & h(4) \end{bmatrix} \begin{bmatrix} v_A(1) \\ v_A(2) \\ v_A(3) \\ v_A(4) \\ \vdots \\ v_A(k_t) \end{bmatrix} \quad (2)$$

According to (1) and (2), the  $k$ -th approximation and wavelet coefficient values are only influenced by the last  $L$  samples of the original signal when  $k \geq L$ . In this paper, the samples of the original signal are obtained in real-time. In this case, the pyramid algorithm of the MODWT could be adapted for real-time and both the approximation and wavelet coefficients soon after each sampling process are given by [14, 15]:

$$A_{v_A}(k) = \sum_{l=1}^L g(l)v_A(k+l-L), \quad (3)$$

$$W_{v_A}(k) = \sum_{l=1}^L h(l)v_A(k+l-L), \quad (4)$$

since  $\exists\{v_A(k-L+1), \dots, v_A(k-1), v_A(k)\}$ . The real-time simulator must be robust enough to solve the network equations and to compute the approximation and wavelet coefficients of all voltages and currents in each simulation time step.

According to the Parseval theorem, the energy of a signal can be decomposed in terms of the energy of the approximation coefficients and the energy of the wavelet coefficients at first scale, as follows [16]

$$\sum_{k=1}^{k_t} |v_A(k)|^2 = \sum_{k=1}^{k_t} |W_{v_A}(k)|^2 + \sum_{k=1}^{k_t} |A_{v_A}(k)|^2, \quad (5)$$

or

$$\mathcal{E} = \dot{\mathcal{E}} + \ddot{\mathcal{E}}, \quad (6)$$

where  $\mathcal{E} = \sum_{k=1}^{k_t} |v_A(k)|^2$ : energy of the signal;  $\dot{\mathcal{E}} = \sum_{k=1}^{k_t} |W_{v_A}(k)|^2$ : wavelet coefficient energy;  $\ddot{\mathcal{E}} = \sum_{k=1}^{k_t} |A_{v_A}(k)|^2$ : approximation coefficient energy.

The real-time approximation and wavelet coefficient energies ( $\ddot{\mathcal{E}}$  and  $\dot{\mathcal{E}}$ ) of a signal (voltage or current), at the first scale, are computed at the sample  $k$  as follows:

$$\ddot{\mathcal{E}}(k) = \sum_{m=k}^{k-\Delta k+1} |A(m)|^2, \quad (7)$$

$$\dot{\mathcal{E}}(k) = \sum_{m=k}^{k-\Delta k+1} |W(m)|^2, \quad (8)$$

since  $\exists\{A(k-\Delta k+1), \dots, A(k-1), A(k)\}$  and  $\exists\{W(k-\Delta k+1), \dots, W(k-1), W(k)\}$ ;  $\Delta k = f_s/f$  is the coefficient amount equivalent to one cycle of the fundamental power frequency ( $f$ ).

According to (7) and (8), in each simulation time step, the energies of a signal are computed considering the last approximation and wavelet coefficients in one cycle (real-time sliding windows).

### 3 Real-Time Transient Disturbance Detection and Classification

#### 3.1 Transmission Line Faults

Faults upon overhead transmission lines are usually characterized by transients soon after both fault inception and clearance times as a consequence of travelling waves [1, 19]. In this paper, the incidence of these transients at monitoring points is called transient inception (TI). Fig. 1 depicts an actual oscillographic record with single-line-to-ground (SLG) fault. This record presents four TIs: pre-fault transients at sample  $k_1$ , fault-induced transients at sample  $k_2$ , transients due to fault clearance at local end at sample  $k_3$ , and transients due to fault clearance at remote end at sample  $k_4$ . The beginning of the  $i^{th}$  TI is located at sample  $k_i$ .

Fig. 2 depicts the wavelet coefficient energies  $\dot{\mathcal{E}}_{v_A}$ ,  $\dot{\mathcal{E}}_{v_B}$ ,  $\dot{\mathcal{E}}_{v_C}$ ,  $\dot{\mathcal{E}}_{i_A}$ ,  $\dot{\mathcal{E}}_{i_B}$ , and  $\dot{\mathcal{E}}_{i_C}$  regarding the fault shown in Fig. 1. The normalized approximation coefficient energies  $\ddot{\mathcal{E}}_{v_A}$ ,  $\ddot{\mathcal{E}}_{v_B}$ ,  $\ddot{\mathcal{E}}_{v_C}$ ,  $\ddot{\mathcal{E}}_{i_A}$ ,  $\ddot{\mathcal{E}}_{i_B}$ , and  $\ddot{\mathcal{E}}_{i_C}$  are shown in Fig. 3.

The wavelet coefficient energies related to steady-state system operation are due to electrical noises and present almost constant values. However, a fast-rising energy occurs at least in one energy waveform regarding each TI. This parameter is used by the proposed method to detect and locate the various TIs in real-time. According to Fig. 2, four TIs could be detected through fast-rising energy variations. At wavelet coefficient energy waveforms, a TI is detected at sample  $k_{iE}$ .

Fig. 4 depicts some binary diagnostic variables used for real-time detection and classification of power system disturbances. The binary variable  $E_{TI}$  indicates the real-time detection of a TI. When a TI is detected at least in one of the wavelet coefficient energies  $\dot{\mathcal{E}}_{v_A}$ ,  $\dot{\mathcal{E}}_{v_B}$ ,  $\dot{\mathcal{E}}_{v_C}$ ,  $\dot{\mathcal{E}}_{i_A}$ ,  $\dot{\mathcal{E}}_{i_B}$ , and  $\dot{\mathcal{E}}_{i_C}$ ,  $E_{TI}$  presents high level ( $E_{TI}=1$ ) during a half-cycle. During this interval, the method does not search for a new TI. The beginning and end time of the fault are identified in real-time when  $E_{TI}=\uparrow$ . In addition, in a case of fault, a minimum of two TIs are detected ( $n_{TI} \geq 2$ ).

The binary variable  $E_{dist}=1$  indicates that the power system operation may be under the influence of transient disturbances. In a case of fault, at least one energy waveform presents values greater than a typical value during the steady-state system operation. According to Figs. 2 and 4,  $E_{dist}=1$  from the first TI detection to the end of the fault.

The binary variable  $E_{DT}=\uparrow$  indicates the end of the disturbance at sample  $k_{iDT}$ . In a case of transmission line fault, at least one phase current tends toward zero after the fault clearance. In this case, the related approximation coefficient energy drops to zero (Fig. 3). During  $E_{dist}=1$ , when  $\ddot{\mathcal{E}}_{i_A}$ ,  $\ddot{\mathcal{E}}_{i_B}$ , or  $\ddot{\mathcal{E}}_{i_C}$  drops to zero,  $E_{DT}=\uparrow$  and  $E_{dist}=\downarrow$ .  $E_{DT}=1$  during the dead time, which has been assumed to be 20 cycles in this paper. The proposed method does not work during  $E_{DT}=1$ , from  $k_{iDT}$  to  $k_{fDT}=k_{iDT}+20\Delta k$ .

According to Fig. 2, the fourth TI (related to the fault clearance at remote end) would be detected by the proposed method. However, during  $E_{DT}=1$ , TIs are not detected.

The approximation coefficient energy analysis is related to the real-time disturbance identification. The binary variables  $E_{pre}$  and  $E_{post}$  indicate the status of the currents just before and soon after the disturbances, respectively. For instance, in a case of fault,  $\dot{\mathcal{E}}_{i_A}$ ,  $\dot{\mathcal{E}}_{i_B}$ , and  $\dot{\mathcal{E}}_{i_C}$  present values according to steady-state system operation. Therefore,  $E_{pre}=1$  after the first TI detection. On the other hand,  $\ddot{\mathcal{E}}_{i_A}$ ,  $\ddot{\mathcal{E}}_{i_B}$ , or  $\ddot{\mathcal{E}}_{i_C}$  present null values soon after the fault clearance. In this case,  $E_{post}=0$  during  $E_{DT}=1$ .

### 3.2 Voltage Sags due to Faults

Voltage sags are short or long duration reductions in rms voltage, caused by faults, overloads, and the starting of large motors [6]. Faults are the main cause of voltage sags in transmission lines, and sags due to other events will not be dealt with in this paper. Fig. 5 depicts an actual oscillographic record with voltage sag due to the SLG fault shown in Fig. 1.

Fig. 6 depicts the wavelet coefficient energies  $\dot{\mathcal{E}}_{v_A}$ ,  $\dot{\mathcal{E}}_{v_B}$ , and  $\dot{\mathcal{E}}_{v_C}$  regarding the voltage sag shown in Fig. 5. The normalized approximation coefficient energies  $\ddot{\mathcal{E}}_{v_A}$ ,  $\ddot{\mathcal{E}}_{v_B}$ , and  $\ddot{\mathcal{E}}_{v_C}$  are shown in Fig. 7 and the binary diagnostic variables are shown in Fig. 8.

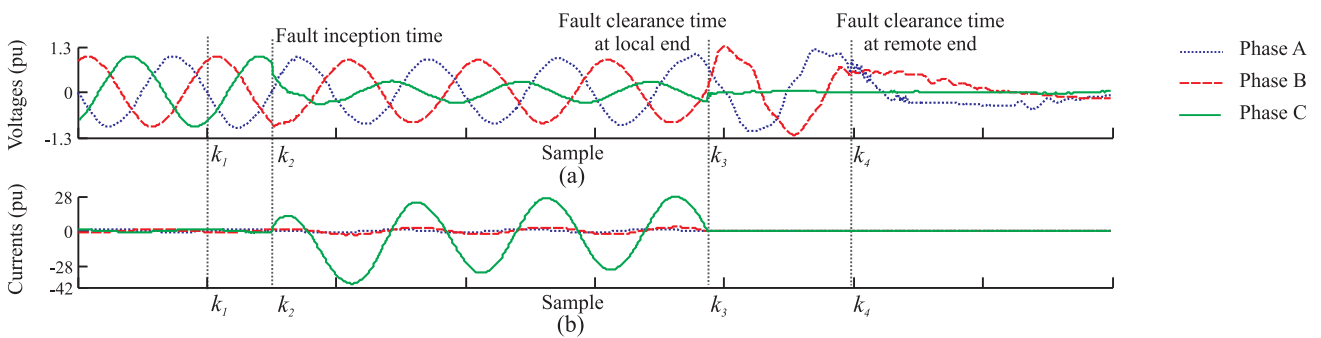


Figure 1: Actual oscillographic record with CG fault: (a) phase voltages; (b) phase currents.

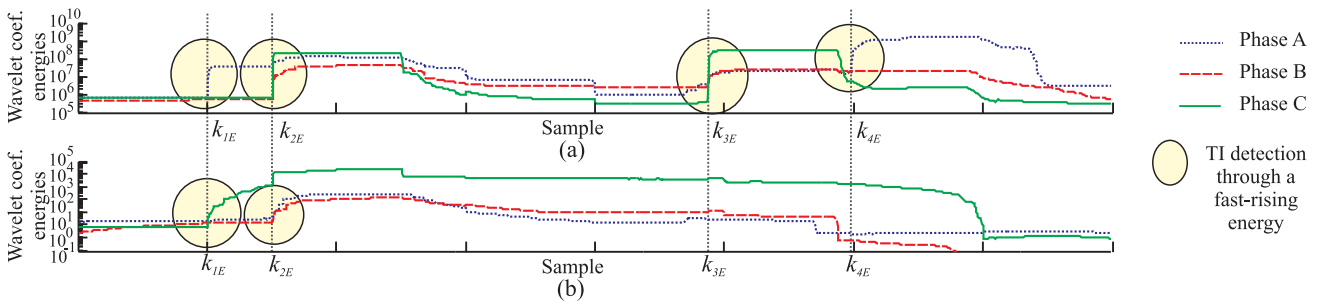


Figure 2: Wavelet coefficient energies: (a)  $\dot{\mathcal{E}}_{v_A}$ ,  $\dot{\mathcal{E}}_{v_B}$ , and  $\dot{\mathcal{E}}_{v_C}$ ; (b)  $\dot{\mathcal{E}}_{i_A}$ ,  $\dot{\mathcal{E}}_{i_B}$ , and  $\dot{\mathcal{E}}_{i_C}$ .

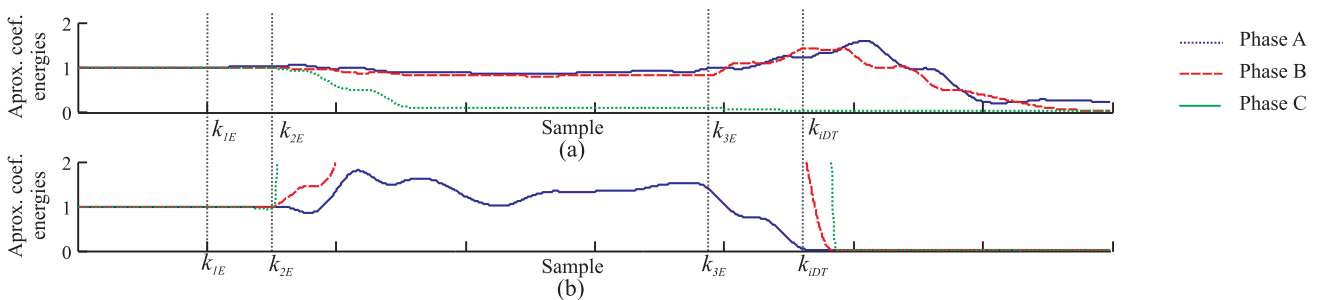


Figure 3: Normalize approximation coefficient energies: (a)  $\ddot{\mathcal{E}}_{v_A}$ ,  $\ddot{\mathcal{E}}_{v_B}$ , and  $\ddot{\mathcal{E}}_{v_C}$ ; (b)  $\ddot{\mathcal{E}}_{i_A}$ ,  $\ddot{\mathcal{E}}_{i_B}$ , and  $\ddot{\mathcal{E}}_{i_C}$ .

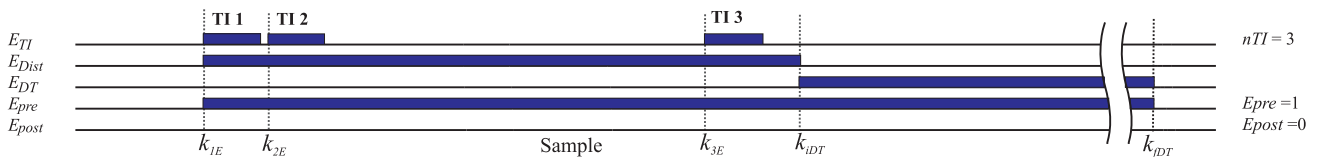


Figure 4: Binary diagnostic variables.

According to Fig. 6, the wavelet coefficient energies related to steady-state system operation were almost constant (at samples  $k < k_{1E}$ ). However, various fast-rising energies were detected at fault inception and clearance time (at samples  $k_{1E}$ ,  $k_{2E}$ ,  $k_{3E}$ , and  $k_{4E}$ ), indicating the beginning and end time of the voltage sag. In addition, in a case of voltage sag due to fault, a minimum of two TIs is detected ( $n_{TI} \geq 2$ ).

In a case of voltage sag, the energies  $\dot{\mathcal{E}}_{i_A}$ ,  $\dot{\mathcal{E}}_{i_B}$ , and  $\dot{\mathcal{E}}_{i_C}$  present values according to steady-state system operation before the fault. In this case,  $E_{pre}=1$  after the first TI detection. After the fault-clearing time, the phase voltages and currents tend to steady-state normal system operation. As a consequence,  $\dot{\mathcal{E}}_{i_A}$ ,  $\dot{\mathcal{E}}_{i_B}$ , and  $\dot{\mathcal{E}}_{i_C}$  present almost constant values. As a consequence,  $E_{pre}=1$  and  $E_{post}=1$  during  $E_{DT}=1$ . When  $E_{post}=1$ , the dead time is only four cycles of fundamental power frequency. After this time, the next TI detection will be associated with a new disturbance.

The binary variable  $E_{sag}$  is used for real-time identification of voltage sags. During  $E_{dist}=1$ , the values of the energies  $\dot{\mathcal{E}}_{v_A}$ ,  $\dot{\mathcal{E}}_{v_B}$ , and  $\dot{\mathcal{E}}_{v_C}$  are compared to the respective

energy value at steady-state system operation (before the first TI detection). For instance, if the energies  $\dot{\mathcal{E}}_{v_A}$ ,  $\dot{\mathcal{E}}_{v_B}$ , and/or  $\dot{\mathcal{E}}_{v_C}$  present values less than 95% of the reference value,  $E_{sag}$  presents high level. In a case of  $E_{sag}=1$  for more than half cycle, a voltage sag is confirmed in real-time.

### 3.3 Transmission Line Energization/De-energization and Switching Transients

A switching operation to energize a transmission line is transient in nature. Therefore, transients can be detected in various power system points. However, the voltages and currents present distinctive features at different monitoring points.

Fig. 9 depicts a simplified transmission system where a transmission line is opened in both terminals. The phase A voltage and current at three distinctive monitoring points and the respective wavelet coefficient energies at the first scale and binary diagnostic variables are also shown in Fig. 9.

According to Fig. 9(b), at switching point, the wavelet coefficient energies present a hard increase and the switch-

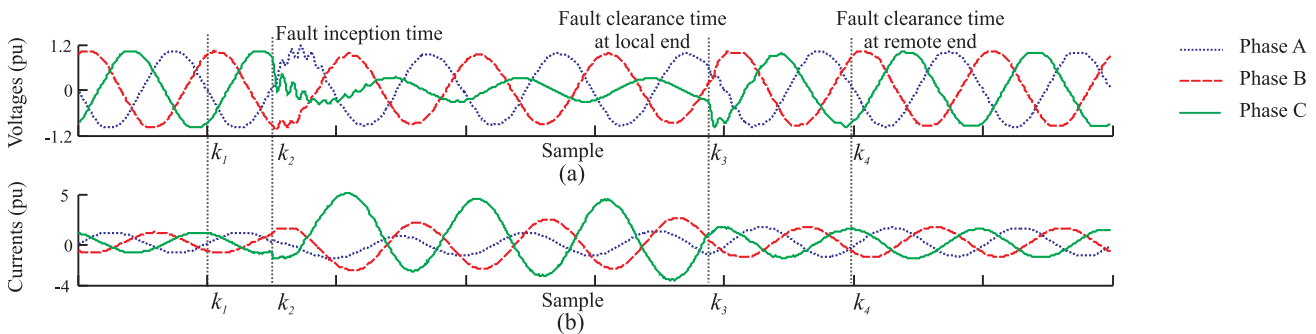


Figure 5: Actual oscillographic record with voltage sag: (a) phase voltages; (b) phase currents.

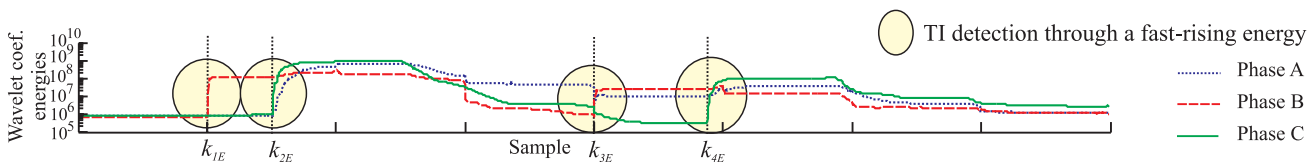


Figure 6: Wavelet coefficient energies:  $\dot{\mathcal{E}}_{v_A}$ ,  $\dot{\mathcal{E}}_{v_B}$ , and  $\dot{\mathcal{E}}_{v_C}$ .

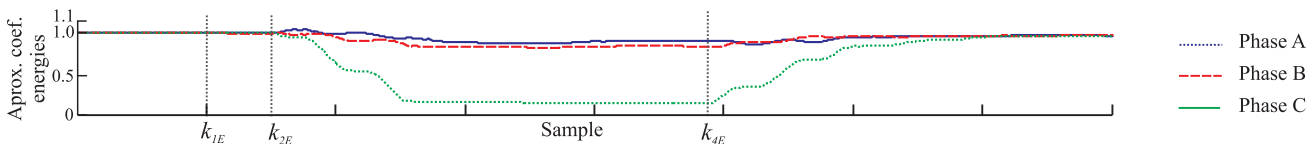


Figure 7: Normalized approximation coefficient energies:  $\ddot{\mathcal{E}}_{v_A}$ ,  $\ddot{\mathcal{E}}_{v_B}$ , and  $\ddot{\mathcal{E}}_{v_C}$ .

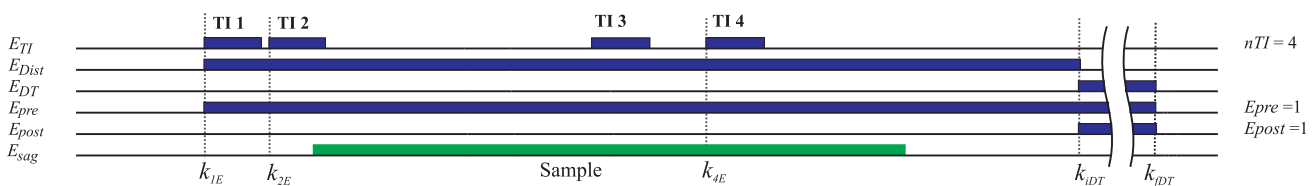


Figure 8: Binary diagnostic variables.

ing operation can be detected in real-time. In this case, the wavelet and approximation coefficient energies of the currents before the switching are null and tend to return to steady-state a few cycles after. As a consequence:  $E_{pre}=0$ ,  $E_{post}=1$ , and  $n_{TI} \geq 1$  when  $E_{DT}=\uparrow$ . This transient disturbance is termed as energization.

The voltages and currents monitored in other power system points far from the switching can also present transients and a disturbance can be detected in real-time. However, these disturbances present different features from energization and are termed as switching transients in this paper. Generally, the wavelet and approximation coefficient energies of the currents before the switching are in steady-state and tend back toward steady-state a few cycles after (Fig. 9(a)). As a consequence:  $E_{pre}=1$ ,  $E_{post}=1$ , and  $n_{TI} \geq 1$  when  $E_{DT}=\uparrow$ . In some cases, the wavelet and approximation coefficient energies of the currents before and after the switching are null (Fig. 9(c)) and  $E_{pre}=0$ ,  $E_{post}=0$ , and  $n_{TI} \geq 1$  when  $E_{DT}=\uparrow$ .

In a case of transmission line de-energization, transients in voltages and currents at switched point are detected as de-energization in real-time with  $E_{pre}=1$ ,  $E_{post}=0$ , and  $n_{TI} \geq 1$  when  $E_{DT}=\uparrow$ . On the other hand, transients in voltages and currents far from the switched point are detected as switching transients in real-time with either  $E_{pre}=1$ ,  $E_{post}=1$ , and  $n_{TI} \geq 1$  when  $E_{DT}=\uparrow$  or  $E_{pre}=0$ ,  $E_{post}=0$ , and  $n_{TI} \geq 1$  when  $E_{DT}=\uparrow$ .

#### 4 Proposed Method

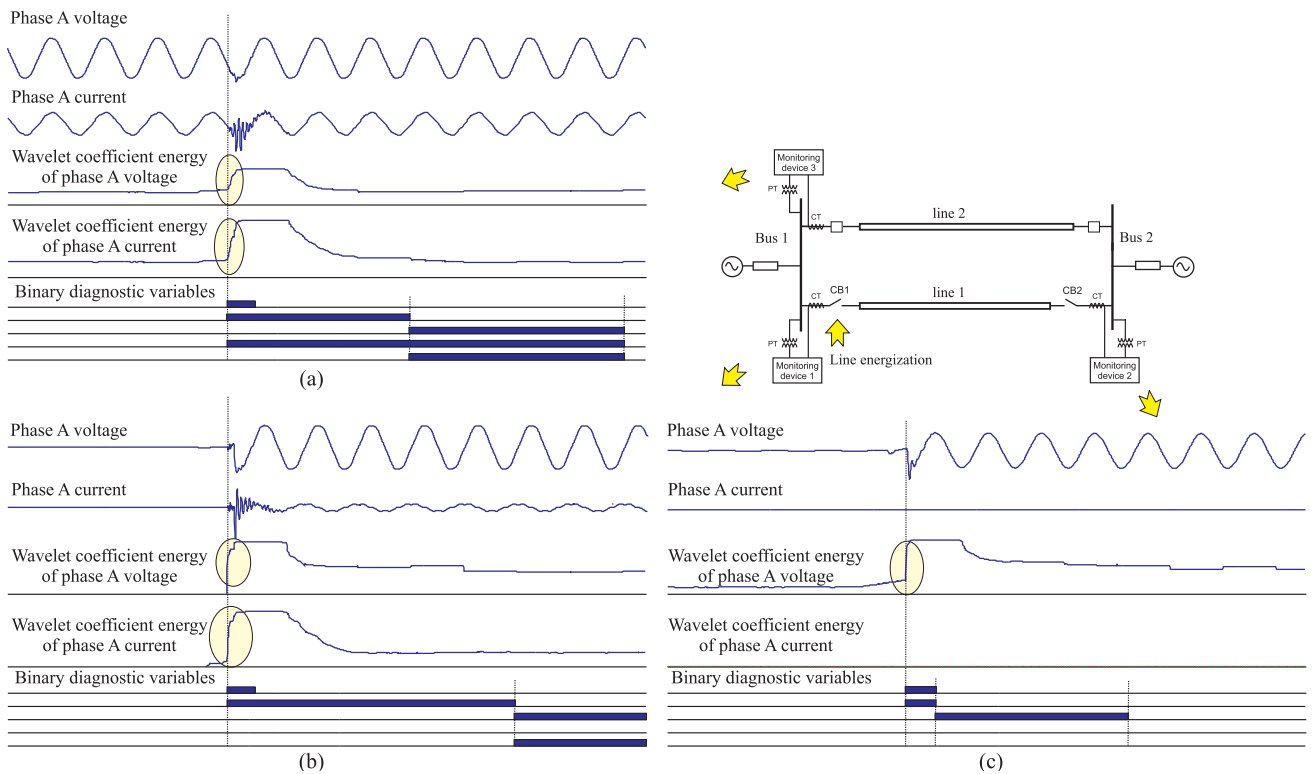
Fig. 10 depicts the simplified flowchart of the proposed real-time disturbance detection and classification. From the simulation time step  $k$ , where the energies can be computed, both wavelet coefficient energies ( $\mathcal{E}_{v_A}$ ,  $\mathcal{E}_{v_B}$ ,  $\mathcal{E}_{v_C}$ ,  $\mathcal{E}_{i_A}$ ,  $\mathcal{E}_{i_B}$ , and  $\mathcal{E}_{i_C}$ ) and approximation coefficient energies ( $\mathcal{E}_{v_A}$ ,  $\mathcal{E}_{v_B}$ , and  $\mathcal{E}_{v_C}$ ) are computed in each time step. The flags  $E_{TI}$ ,  $E_{dist}$ ,  $E_{DT}$ ,  $E_{sag}$ ,  $E_{pre}$ , and  $E_{post}$  are modified in real-time as addressed in the previous section.

The disturbances can be identified in real-time according to the parameters summarized in Tab 1.

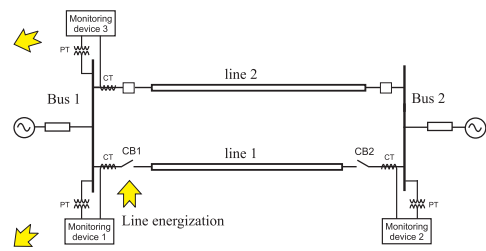
#### 5 Proposed Method Performance Evaluation

In order to evaluate the performance of the proposed disturbance detection method in real-time simulations, the system model depicted in Fig. 11 was modeled by using the RTDS. This system is based on the model proposed by [20]. Each 230 kV transmission line is 45 miles long.

A total of 1000 faults on line 1 was simulated in real-time, each one with random values of fault resistance  $r_f \in \{0, 100\} \Omega$ , fault inception angle  $\theta_f \in \{0^\circ, 180^\circ\}$ , and fault location  $d_f \in \{15, 68\}$  km from bus 1. With regard to the fault type, 67% were SLG faults, 25% were LL faults, 3% were DLG faults, and 5% were three-phase faults [21]. The fault-clearing time in each simulation was about 50 ms (3 cycles of 60 Hz).



**Figure 9:** Transients due to a transmission line energization with opened remote terminal. Monitoring device at: (a) parallel transmission line; (b) switched point; (c) remote terminal of switched line.



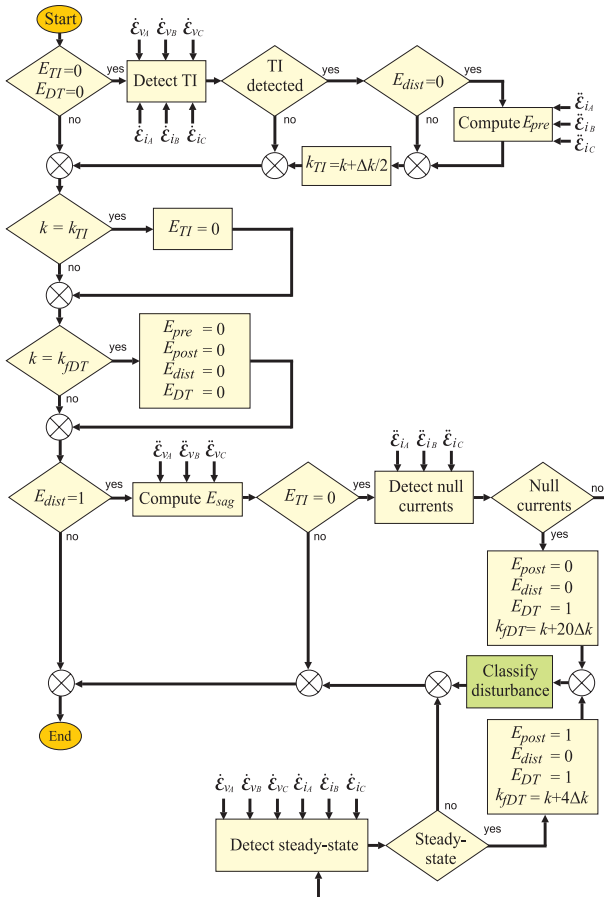


Figure 10: Flowchart of the real-time detection method.

According to Fig. 11, for each fault simulation, the proposed method was simultaneously evaluated at four distinctive points (at both terminals of lines 1 and 2). At line 1, the method must detect a transmission line fault at both ends in real-time. On the other hand, at line 2, the method must detect a voltage sag at both ends in real-time. The disturbance detection method was evaluated in 2000 real-time simulations.

Table 1: Parameters used for real-time disturbance classification.

Disturbance	Parameters			
	$E_{pre}$	$E_{post}$	$n_{PT}$	$E_{sag}$
fault	1	0	$>1$	-
Voltage sag	1	1	$>1$	1
Energization	0	1	$=1$	-
De-energization	1	0	$=1$	-
Switching transients	1	1	$=1$	0

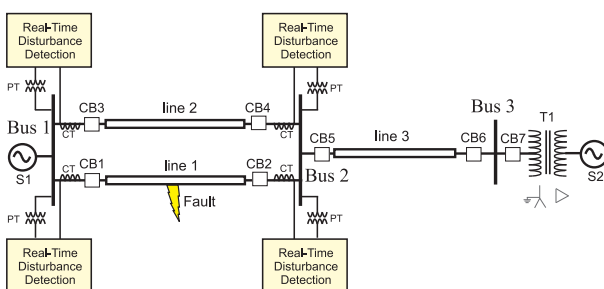


Figure 11: Power system model proposed by [20].

Fig. 12 depicts the voltages and currents at both ends of the line 1 and at line 2 - bus 1, during a real-time fault simulation on line 1, with the following parameters:  $\theta_f=26.8^\circ$ ,  $r_f=12.8 \Omega$  e  $d_f=27$  km from bus 1. The binary parameters used for disturbance detection in real-time are also shown in Fig. 12.

According to Fig. 12, transients regarding the fault inception and clearance time were all detected in real-time ( $E_{TI}=\uparrow$ ). The disturbances seen from terminals of line 1 were classified as fault ( $E_{pre}=1$  and  $E_{post}=0$  in  $E_{DT}=\uparrow$ , with  $n_{TI}=2$  in Figs. 12(a) and 12(b)). On the other hand, the disturbance seen from the bus 1 terminal of line 2 was classified as voltage sag ( $E_{pre}=1$  and  $E_{post}=1$  in  $E_{DT}=\uparrow$ , with  $n_{TI}=2$  and  $E_{sag}=1$  in Fig. 12(c)). The dead-time in all cases was adjusted to be 4 cycles in real-time simulations.

The proposed method performance evaluation is summarized in Tab. 2. In all monitoring points, the method detected transients in all real-time simulation and a success rate of 100% was obtained in disturbance detection.

The transients at monitoring points in line 1 regarding the fault inception were not detected in 11 real-time simulations. In these cases, the faults were classified as transmission line de-energizations and a success rate of 98.90% was obtained in disturbance classification. With regard to monitoring points in line 2, all disturbances were classified as voltage sags.

Table 2: Proposed method performance evaluation during real-time fault simulation on line 1.

monitoring line	Amount of simulations	Success rate at disturbance detection	Success rate at disturbance classification
line 1 - bus 1	1000	100%	98.90%
line 1 - bus 2	1000	100%	98.90%
line 2 - bus 1	1000	100%	100%
line 2 - bus 2	1000	100%	100%

A total of 1000 faults was also simulated in real-time on line 3 (Fig. 13), each one with random values of fault resistance  $r_f \in \{0, 100\} \Omega$ , fault inception angle  $\theta_f \in \{0^\circ, 180^\circ\}$ , and fault location  $d_f \in \{15, 68\}$  km from bus 3. In these simulations, the proposed method was simultaneously evaluated at four distinctive points. With regard to the fault type, 67% were SLG faults, 25% were LL faults, 3% were DLG faults, and 5% were three-phase faults [21]. The fault-clearing time in each simulation was about 50 ms (3 cycles of 60 Hz).

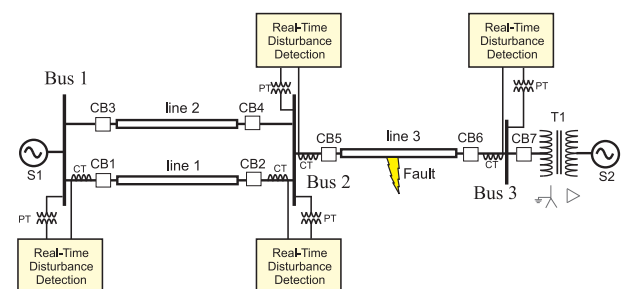
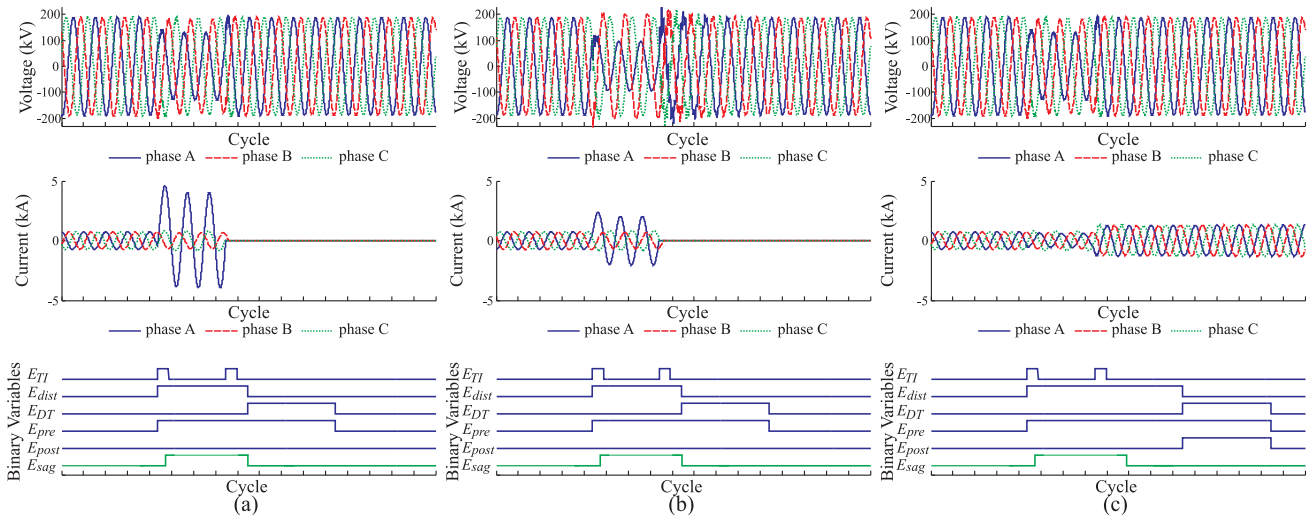


Figure 13: Power system model proposed by [20].



**Figure 12:** Voltages, currents and diagnostic variables for real-time disturbance analysis. Monitoring point at: (a) line 1 - bus 1; (b) line 1 - bus 2; (c) line 2 - bus 1.

The proposed method performance evaluation is summarized in Tab. 3. In all monitoring points, the method detected transients in all real-time simulation and a success rate of 100% was obtained in disturbance detection.

The transients at monitoring points at busses 2 and 3 (line 3), regarding the fault inception were not detected in 12 and 11 real-time simulations, respectively. In these cases, the faults were classified as transmission line de-energizations and a success rate of 98.80% and 98.90% were obtained in disturbance classification at busses 2 and 3, respectively. With regard to monitoring points on line 1, all disturbances were classified as voltage sags.

**Table 3:** Proposed method performance evaluation during real-time fault simulation on line 3.

monitoring line	Amount of simulations	Success rate at disturbance detection	Success rate at disturbance classification
line 3 - bus 3	1000	100%	98.80%
line 3 - bus 2	1000	100%	98.90%
line 1 - bus 1	1000	100%	100%
line 1 - bus 2	1000	100%	100%

## 6 Conclusions

This paper presented the wavelet and approximation coefficient energies as tools for detection of faults and power system disturbances with transients. The distinctive feature of the proposed wavelet-based method is the ability to detect and classify the disturbances in real-time.

The method was evaluated 8000 times in real-time simulations. All disturbances were detected in real-time and a success rate of 99.44% was obtained in real-time disturbance identification.

The proposed method provided meaningful disturbance detection in real-time simulations and it will be further implemented into a digital signal processor in order to detect disturbances in real applications.

## 7 Acknowledgement

This work was supported by the Brazilian National Research Council (CNPq).

## REFERENCES

- [1] G. W. Swift, "The spectra of fault-induced transients," *IEEE Transactions on Power Apparatus and Systems*, vol. PAS-98, no. 3, pp. 940–947, May 1979.
- [2] A. T. Johns, R. K. Aggarwal, and Z. Q. Bo, "Non-unit protection technique for ehv transmission systems based on fault-generated noise," *IEE Proc. Gener. Transm. Distrib.*, vol. 141, no. 2, pp. 133–140, March 1994.
- [3] S. Santoso, E. J. Powers, W. M. Grady, and P. Hofmann, "Power quality assessment via wavelet transform analysis," *IEEE Transactions on Power Delivery*, vol. 11, no. 2, pp. 924–930, April 1996.
- [4] W. A. Wilkinson and M. D. Cox, "Discrete wavelet analysis of power system transients," *IEEE Transactions on Power Systems*, vol. 11, pp. 2038–2044, Nov 1996.
- [5] S. A. Probert and Y. H. Song, "Detection and classification of high frequency transients using wavelet analysis," *Proc. 2002 IEEE Power Engineering Society Summer Meeting*, vol. 2, pp. 801–806, Chicago, USA, July 2002.
- [6] M. H. J. Bollen and I. Y.-H. Gu, *Signal Processing of Power Quality Disturbances*. New York, USA: IEEE, 2006.

- [7] F. B. Costa, K. M. Silva, K. M. C. Dantas, B. A. Souza, and N. S. D. Brito, "A wavelet-based algorithm for disturbances detection using oscillographic data," *International Conference on Power Systems Transients*, Lyon, France, jun 2007.
- [8] O. Gencer, S. Öztürk, and T. Erfidan, "A new approach to voltage sag detection based on wavelet transform," *Electrical Power and Energy Systems*, pp. 133–140, jul 2009.
- [9] F. B. Costa, B. A. Souza, and N. S. D. Brito, "Detection and classification of transient disturbances in power systems," *IEEJ Trans. PE*, pp. 910–916, Oct 2010.
- [10] O. A. S. Youssef, "Fault classification based on wavelet transforms," *Transmission and Distribution Conference and Exposition*, vol. 1, pp. 531–536, Nov 2001.
- [11] K. M. Silva, B. A. Souza, and N. S. D. Brito, "Fault detection and classification in transmission lines based on wavelet transform and ann," *IEEE Transactions on Power Delivery*, vol. 21, no. 4, pp. 2058–2063, Oct 2006.
- [12] D.-J. Zhang, Q. H. Wu, Z. Q. Bo, and B. Counce, "Transient positional protection of transmission lines using complex wavelets analysis," *IEEE Transactions on Power Delivery*, vol. 18, no. 3, pp. 705–710, jul. 2003.
- [13] S. P. Valsan and K. Swarup, "Wavelet transform based digital protection for transmission lines," *International Journal of Electrical Power & Energy Systems*, vol. 31, no. 7-8, pp. 379–388, 2009.
- [14] F. B. Costa, "Uma técnica de diagnóstico em tempo real de distúrbios transitórios baseada na transformada wavelet para uso em registradores digitais de perturbação," Ph.D. dissertation, Federal University of Campina Grande, Campina Grande, Brazil, 2010.
- [15] F. B. Costa, B. A. Souza, and N. S. D. Brito, "Real-time detection of fault-induced transients in transmission lines," *IET Electronics Letters*, pp. 753–755, May 2010.
- [16] D. B. Percival and A. T. Walden, *Wavelet Methods for Time Series Analysis*. New York, USA: Cambridge University Press., 2000.
- [17] I. Daubechies, *Ten Lectures on Wavelets*. Philadelphia, USA: CBMS-NSF Regional Conference Series, SIAM, 1992.
- [18] C. H. Kim and R. Aggarwal, "Wavelet transform in power system: Part 2 examples of application to actual power system transients," *Power Engineering Journal*, pp. 193–202, August 2001.
- [19] A. A. Girsis and R. G. Brown, "Modelling of fault-induced noise signals for computer relaying applications," *IEEE Transactions on Power Apparatus and Systems*, vol. PAS-102, no. 9, pp. 2834–2841, Sep 1983.
- [20] *EMTP Reference Models for Transmission Line Relay Testing*, IEEE Power System Relaying Committee, Available on: <http://www.pes-psrc.org/Reports/d6report.zip>, 2004.
- [21] *IEE. Power System Protection - Volume 1: Principles and Components*, IEE, London, United Kingdom: The Institution of Electrical Engineers., 1995.